Journal of Medicinal and Nanomaterials Chemistry 4 (2020) 300-312

SPC

Journal of Medicinal and Nanomaterials Chemistry

Journal homepage: https://jmnc.samipubco.com/

Orginal Research Article

Photocatalytic degradation of industrial pigments by mil-125 derived porous Titanium Dioxide (TiO_2) nanoparticles

Vahid Sabaghi[a], Maisam Jalaly[b,*], Fatemeh Rahnemaye Rahsepar[a]

[a] *School of Chemistry, College of Science, University of Tehran, Tehran, Iran*

[b] *Nanotechnology Department, School of Advanced Technologies, Iran University of Science & Technology (IUST), Tehran, Iran*

ARTICLE INFORMATION

Received: 12 May 2020
Received in revised: 13 July 2020
Accepted: 1 August 2020
Available online: 26 August 2020

DOI: 10.48309/JMNC.2020.4.4

KEYWORDS

Metal-organic framework
Titanium dioxide
Optical properties
Photocatalytic properties

ABSTRACT

Nowadays, metal-organic framework (MOF)-derived porous metal oxide nanoparticles (NPs) has attracted a great attention for remediation of environmental contamination. This work discussed the synthesis approach of the porous and single-phase TiO_2 NPs *via* the thermal treatment of MIL-125 (Ti) at various temperatures. The influences of temperature on the single-phase synthesis and degree of crystallinity of this nanomaterial were investigated. It was revealed that 500 °C was the optimum temperature for the synthesis of anatase phase of nano-titania. The TiO_2 NPs produced by heat-treating at 500 °C was found to have a mean particle size of less than 10 nm, specific surface area of 163 m^2g^{-1}, and pore volume of 0.374 cm^3g^{-1}. The optical properties of the anatase phase of TiO_2 were examined and the value of its indirect energy gap (or band gap) was obtained to be 3.08 eV. High specific surface area and porous structure of the anatase TiO_2 made it a suitable candidate for the photocatalyst agent. This is due to the fact that it increases the loading capacity of the organic pigments and prolongs the light exposure duration. As-synthesized TiO_2 NPs exhibited a high photocatalytic performance for removal of methylene blue (MB), methylene orange (MO) and reactive blue 21 (RB21) organic pigments.

Corresponding author, email: maisam_jalaly@iust.ac.ir (M. Jalaly).
Tel.: +982173225838.

Graphical Abstract

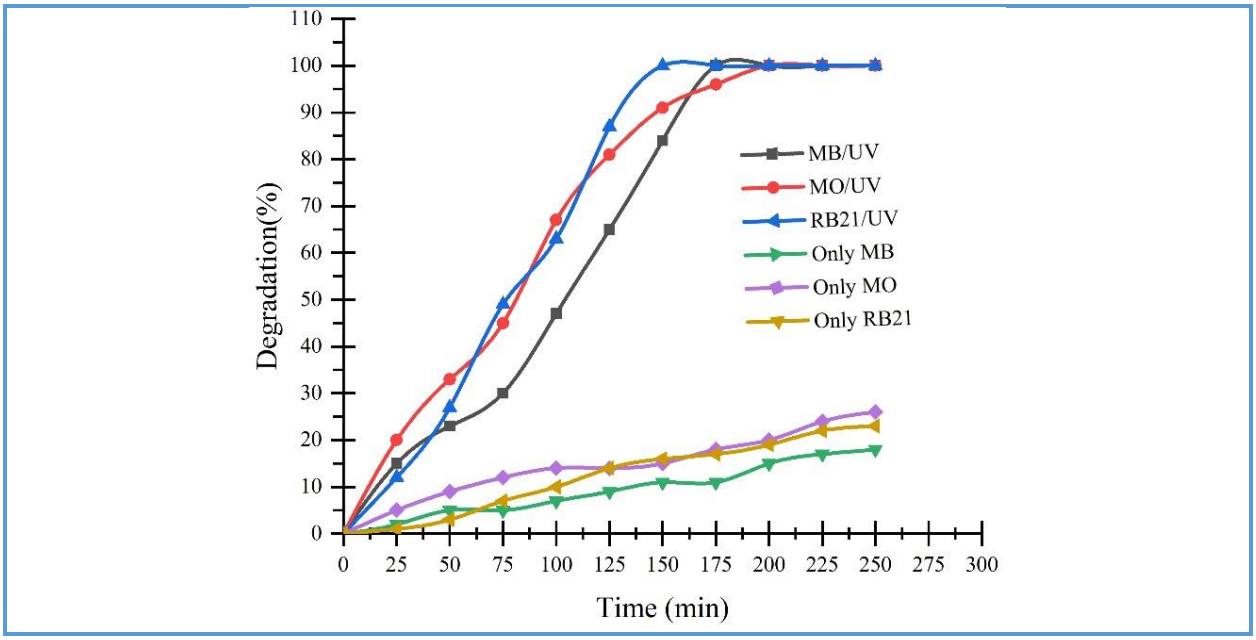

Introduction

Metal-organic frameworks (MOFs) are the practical and novel class of reticular chemicals with periodic network structure. MOFs have direct and indirect extensive applications in many fields including photocatalysts [1], CO_2 capture [2], battery materials [3], supercapacitors [4], chemo-thermal therapy [5], separation agents [6, 7], biosensors [8], and antibacterial agents [9]. Due to using various organic linker and secondary building units (SBUs), a wide range of these compounds has been synthesized for specific purposes [10–13]. MOFs can also be used as a template or intermediate to obtain nano-sized metallic oxides [13–15]. Owing to their high surface area and porosity, MOFs-derived porous NPs have a great potential to be employed as catalysts/photocatalysts [16–18]. It should be noted that several parameters affect the morphology including nanowires, nanotubes, nanocubes, nanospheres, nanorods, and nanosheets, of the metal oxide derived from MOFs [19–23].

Of all the metal oxides, TiO_2 is one of the most popular candidates of semiconducting which can be obtained from MOF structures [24]. TiO_2 has various applications in biotechnology, solar cell, energy storage, catalyst, CO_2 reduction, and hydrogen production [25–30]. TiO_2 exists in three crystalline forms: brookite with the orthorhombic unit cell, anatase and rutile with tetragonal structure [31]. Compared to other photocatalysts such as α-Fe_2O_3, WO_3, ZnO, CuS and ZnS, TiO_2 is widely used because of its economic cost and chemical and biological resistance [32–34]. The bandgap of TiO_2 is usually more than 3 eV (~2.8-3.0 eV for rutile phase and ~3-3.4 eV for anatase phase), thus it is considered as a vigorous photocatalyst for the UV light [35]. Controlling the synthesis parameters for production of nano-scale titanium oxide is very critical, because they can directly affect the optical and photocatalytic behavior of this compound [36, 37].

In the current study, single-phase porous titanium oxide nanoparticles were synthesized from MIL-125(Ti) metal-organic framework or coordination polymer. The optimum

temperature for the synthesis of single-phase TiO_2 nanoparticles from MIL-125 intermediate was assessed, and the optical and photocatalytic properties of the nanoparticles were investigated with a focus on the removal of industrial pigments. The influences of the primary morphology of MIL-125 on the phase transition were discussed, as well.

Experimental

Material and methods

Titanium isopropoxide (TIP, Aldrich, 99.8%), *N,N*-dimethylformamide (DMF, Aldrich 99%), anhydrous methanol (Aldrich, 99.8%), 1, 4-benzene dicarboxylic acid (H_2BDC, Aldrich, 99%) were purchased and used without further purification.

Synthesis of MIL-125(Ti)

MIL-125(Ti) was prepared by the approach reported by Wang *et al.* [38]. For this goal, 2.0 g H_2BDC, 5 mL anhydrous methanol, 45 ml anhydrous DMF and 1.56 mL of TIP were mixed at ambient temperature. The mixture was then transferred to a Teflon-lined autoclave and heated at 150 °C for 16 h. The resulting white-yellow suspension of MIL-125(Ti) was filtered and washed 3 times under stirring with 20 mL anhydrous methanol for 30 min to remove all unreacted organic linkers, then dried at 150 °C. The product of this step is known as inactivated MIL-125(Ti) (MIL-125 with solvent molecules in their pores). Inactivated MIL-125(Ti) was heat-treated at 200 °C under vacuum for 5 h to remove solvent molecules trapped in the pores. The final product of this step is known as activated MIL-125(Ti) (MIL-125 with empty pores). Figure 1 illustrates the schematic procedure for the synthesis of MIL-125(Ti) and TiO_2 nanoparticles.

Synthesis of porous TiO_2 NPs

To prepare the oxide nanophase, activated MIL-125(Ti) was collected and annealed in the furnace. Four annealing temperatures (400, 450, 500, and 550 °C) were evaluated to achieve the optimum temperature which is necessary for the preparation of the single-phase porous titanium oxide. At each temperature, a certain amount of the synthesized MOF was heated for 5 h at a rate of 10 °C/min under the continuous air flow. After cooling down, porous TiO_2 NPs were collected (Figure 1).

Photocatalyst test

This test was used to evaluate the ability of porous TiO_2 NPs as a photocatalyst. 20 mg of porous TiO_2 photocatalyst was separately dispersed in 70 mL of 20 ppm aqueous solutions of methylene blue (MB), methylene orange (MO), and reactive blue 21 (RB21) under stirring. Then, the solutions were exposed to a UV lamp with a power of 400 W. The absorption spectra were measured by the UV-vis double beam PC scanning spectrophotometer in the range of 200-800 nm and finally, photocatalytic activity of porous TiO_2 NPs was evaluated.

Characterization equipment

The Fourier-transform infrared (FT-IR) spectroscopy of porous TiO_2 nanoparticles was performed by an IR 550 spectrometer using KBr pellets. A PANanalytical X'Pert diffractometer with Cu K_α (λ=0.15406 nm) was used for X-ray diffraction (XRD) analysis of MIL-125(Ti) and porous TiO_2. The ultraviolet-visible spectrum was obtained by a UV-vis double beam spectrophotometer (model UVD-2950). Fluorescence measurement was recorded on the RF-5301PC spectrofluorometer. The specific surface area was determined by Brunauer, Emmett and Teller (BET) analysis (Belsorp mini II model, Japan). Field emission

scanning electron microscopy (FE-SEM, Hitachi S-4800) and transmission electron microscopy (TEM- Philips EM 208S) were accomplished to check the morphology of the particles. Thermogravimetric (TG) analysis of activated MIL-125 was carried out by a NETZSCH STA 449C analyzer (Germany) with a heating rate of 10 °C/min under a flow of nitrogen.

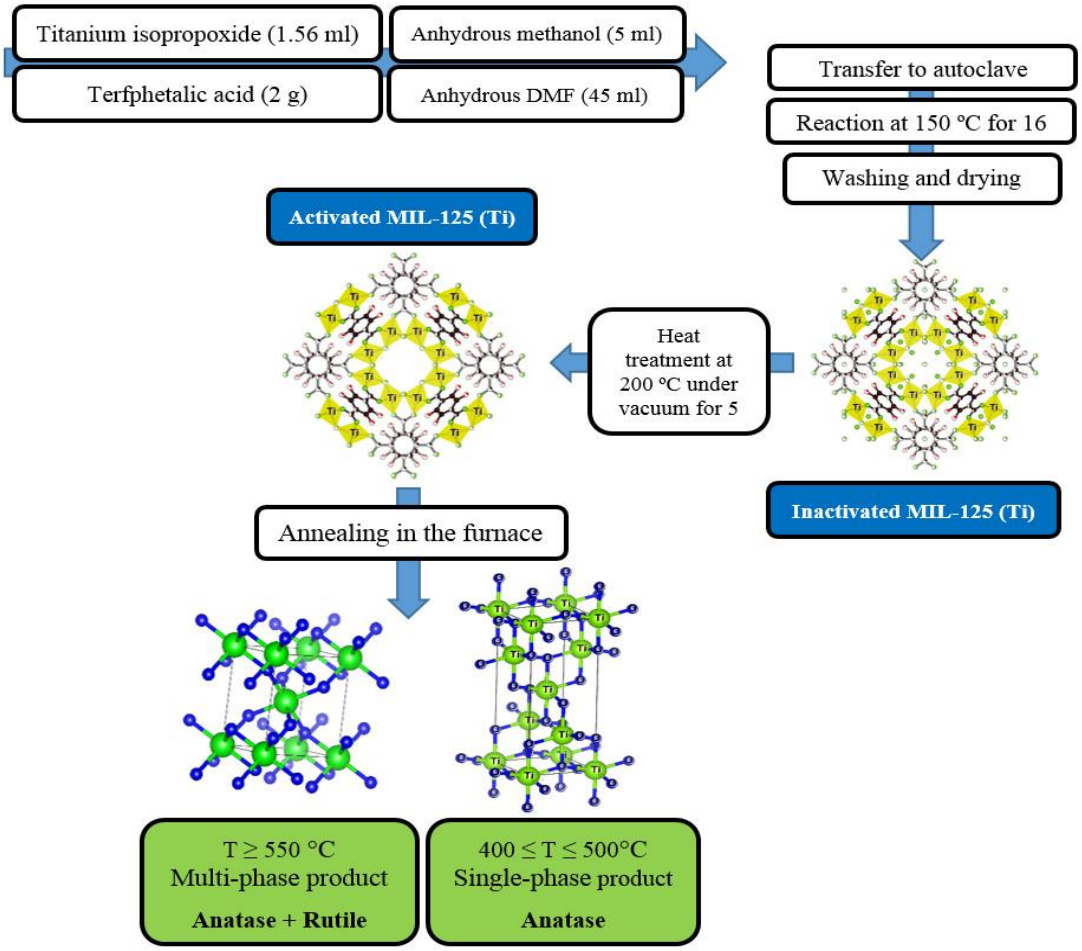

Figure 1. Schematic illustration of synthesis route for MIL-125(Ti) and TiO_2 NPs

Results and Discussion

The FTIR spectra of MIL-125 and TiO_2 are demonstrated in Figure 2 to support the formation of TiO_2 NPs. It is easy to recognize the intense broadband around the 3350 cm^{-1} in both spectra, that is related to asymmetric and symmetric stretching vibrations of hydroxyl groups connected to the surfaces of MIL-125 (Ti) and TiO_2 NPs [39, 40]. It should be noted that this characteristic band in the MOF located at the range of 3300-3500 cm^{-1} may be assigned to the free solvent molecules trapped in the pores [41]. The stretching vibration of Ti-O-Ti and O-Ti-O due to the inter-atomic interaction is often observed at 400–1250 cm^{-1} in the FTIR spectrum [42–44]. The sharp spectroscopic band at 1400 and 1530 cm^{-1} are attributed to the carboxylate groups as a linker in the MOF structure [45–47]. TiO_2 has a small peak at 1630 cm^{-1}, which is representative of the adsorbed H_2O molecule [48].

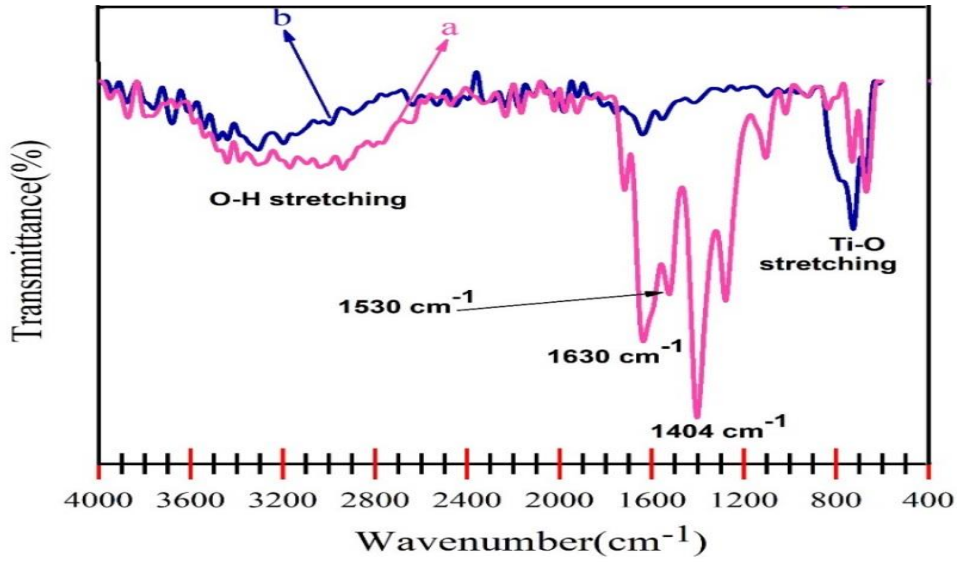

Figure 2. FT-IR analysis of (a) MIL-125(Ti) and (b) TiO_2 nanoparticles.

Figure 3 represents the result of TG analysis for MIL-125(Ti). The weight loss at the range of 45–100 °C (~10%) is related to the removal of methanol molecules as a solvent trapped in the pores of the MOF [49]. The second characteristic weight loss occurred at the range of 100–350 °C (~14%) is attributed to the elimination of DMF guest molecule as a solvent [47]. Finally, the major weight loss at the range of 350–525 °C (~20%) corresponds to the structural conversion of MIL-125 into titanium oxide NPs [49]. The derivative thermogravimetry (DTG) curve was also plotted along with the TG graph (Figure 3). DTG is usually used to simplify the recognition of the temperature range of the weight loss when the peaks of the TG curve are close together.

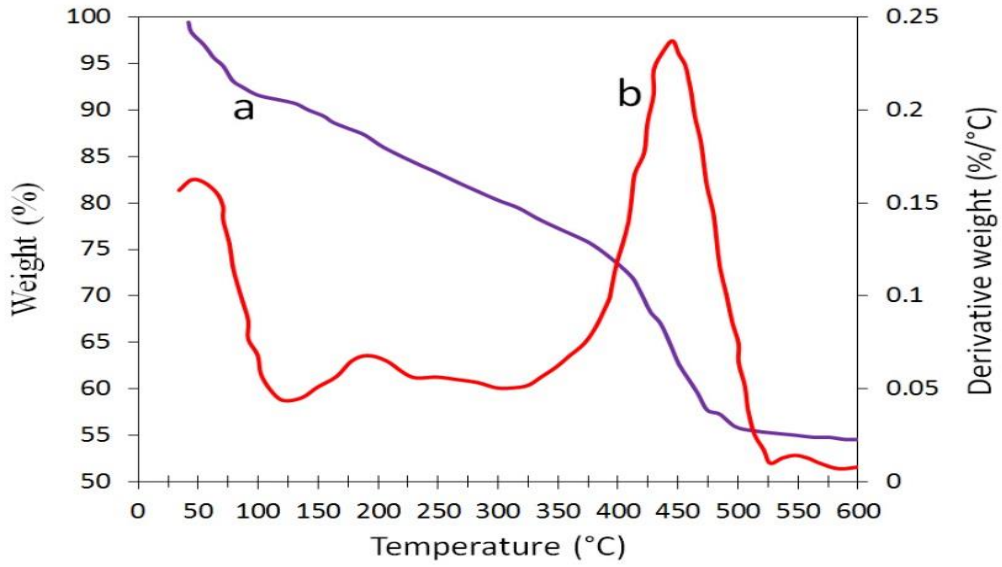

Figure 3. a) Thermogravimetric (TG) and b) derivative thermogravimetric (DTG) curves of MIL-125(Ti)

Figure 4a illustrates the X-ray diffraction (XRD) of the MIL-125(Ti) synthesized in the autoclave, which is in agreement with the patterns reported earlier [50, 51]. Figure 4b demonstrates the XRD patterns of TiO_2 samples obtained from the heat treatments of MIL-125 at different temperatures (400–550 °C). The rutile and anatase phases can be clearly detected from XRD patterns. The major peaks in the patterns of the samples annealed at 400–500 °C belong to the anatase phase of TiO_2 [38, 43]. As seen in Figure 4b, the phase transformation (anatase to rutile) begins when the temperature increases to 550 °C. Formation of the rutile phase could be completed as the annealing temperature is increased further. By increasing the temperature from 400 °C to 500 °C, the degree of crystallinity of the TiO_2 anatase phase increased, arising from the increase in the intensity of all the peaks. On the other hand, a small amount of the rutile phase was observed at 550 °C. This demonstrated that the increase in the temperature higher than 500 °C resulted in the formation of multi-phase TiO_2 NPs [41]. Therefore, the optimum temperature for the synthesis of high-crystalline, single-phase, anatase TiO_2 was 500 °C.

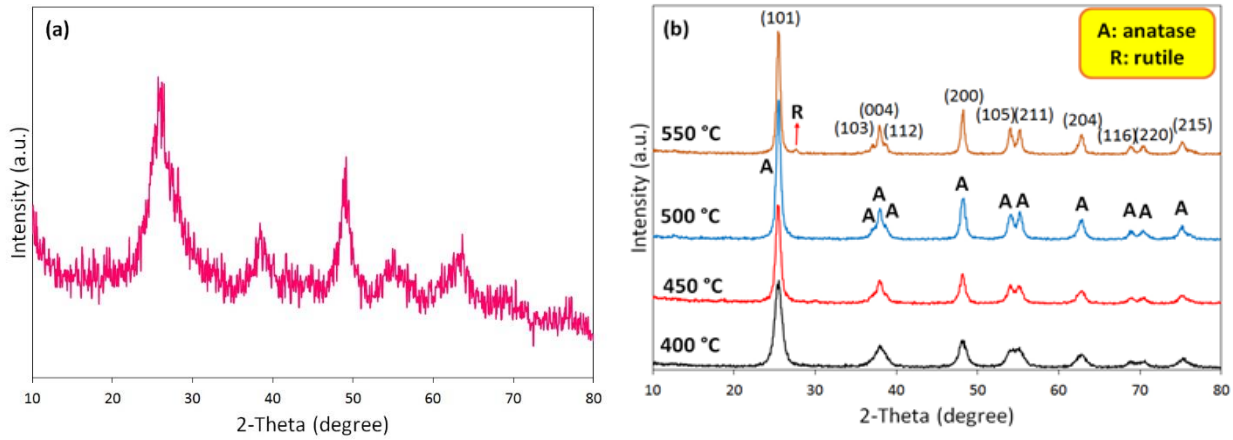

Figure 4. XRD patterns of a) MIL-125(Ti) and b) TiO_2 nanoparticles prepared at different temperatures.

Ultraviolet-visible spectroscopy can be used to recognize the functional groups or confirm the structure of the materials. Figure 5a shows the UV-vis spectrum of the synthesized TiO_2 nanoparticles. Since the maximum absorption of TiO_2 occurred at the wavelength of 364 nm (in the UV range of electromagnetic radiation, 10-400 nm), TiO_2 is reasonably expected to be a UV active photocatalyst. Moreover, photoluminescence (PL) spectroscopy is a non-contact and nondestructive approach for the identification of the electronic structure of materials. The photoluminescence (PL) emission spectrum of TiO_2 NPs upon irradiation with the ultraviolet radiation of the wavelength λ = 380 nm is shown in Figure 5b. It is obvious that the PL maximum intensity (λ_{em}) occurred at 543 nm. This emission is due to the de-excitation from lower vibration states in the oxygen vacancies of TiO_2 lattice to the ground state [52]. Figure 5c depicts the Tauc plot for TiO_2 nanoparticles, which is a high-sensitivity method for measuring the bandgap of semiconductors. TiO_2 is a semiconductor, and any semiconductor can be a direct/indirect-bandgap one. Anatase and brookite phases of TiO_2 have an indirect bandgap, while rutile has the direct band gap [53]. Using the

extrapolation of the Tauc plot, the optical indirect bandgap of the synthesized anatase phase of TiO_2 NPs was calculated to be 3.08 eV.

Figure 6 illustrates the FE-SEM images of the MIL-125 (a) and porous TiO_2 NPs (c). A semi-spherical metal-organic framework with an average diameter of 6.72 nm was successfully synthesized. Figure 6c displays the spherical morphology of TiO_2 particles with an average diameter of 8.95 nm prepared from the heat treatment of MIL-125 at 500 °C for 5 h. The histograms of MIL-125 (b) and TiO_2 (d) shown in Figure 6 demonstrates a narrow distribution particle size under 10 nm, although agglomeration of nanoparticles can be detected in both cases.

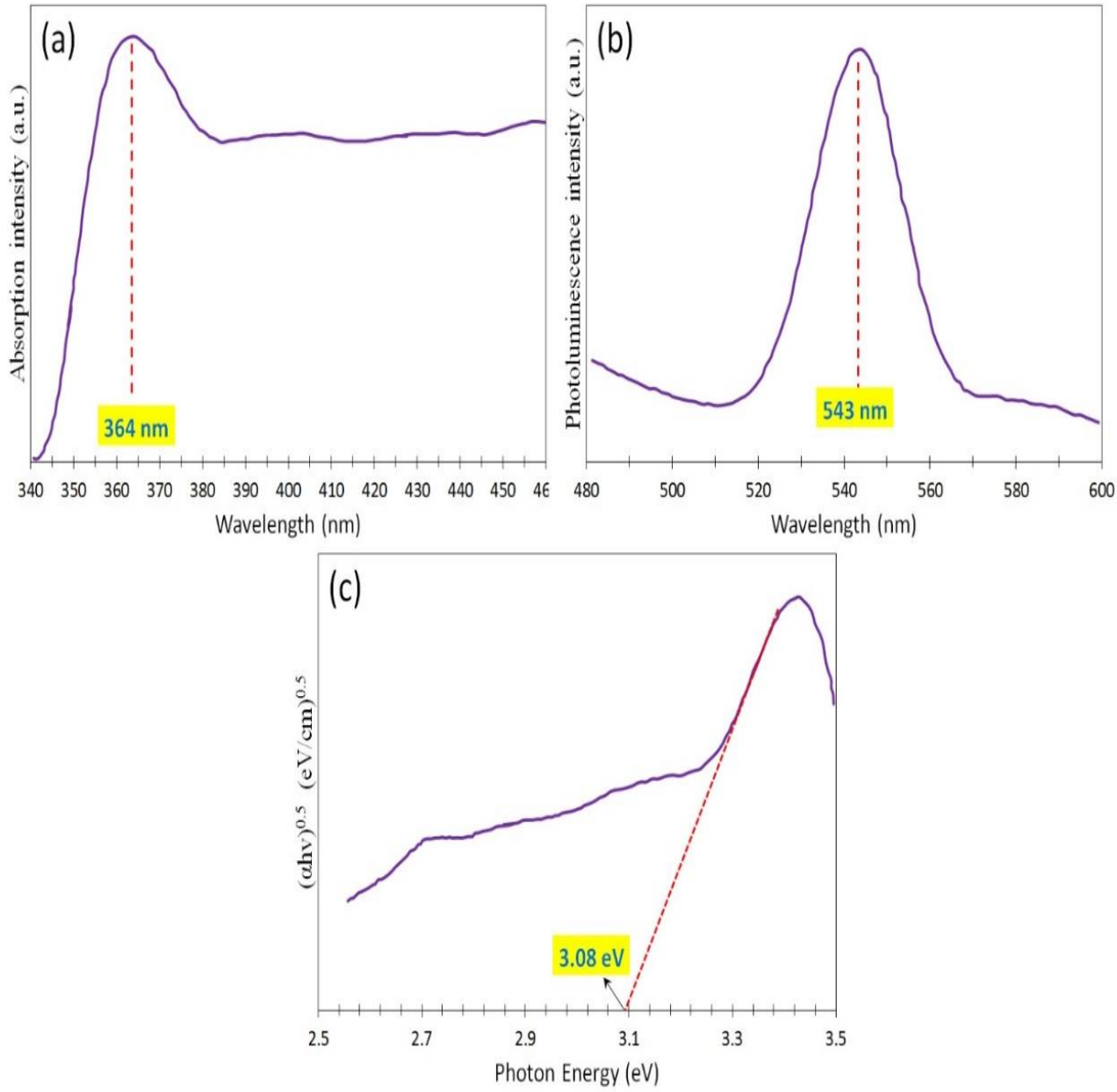

Figure 5. a) UV-visible spectrum, b) photoluminescence spectrum, and c) Tauc plot for obtaining indirect band gap of TiO_2 nanoparticles.

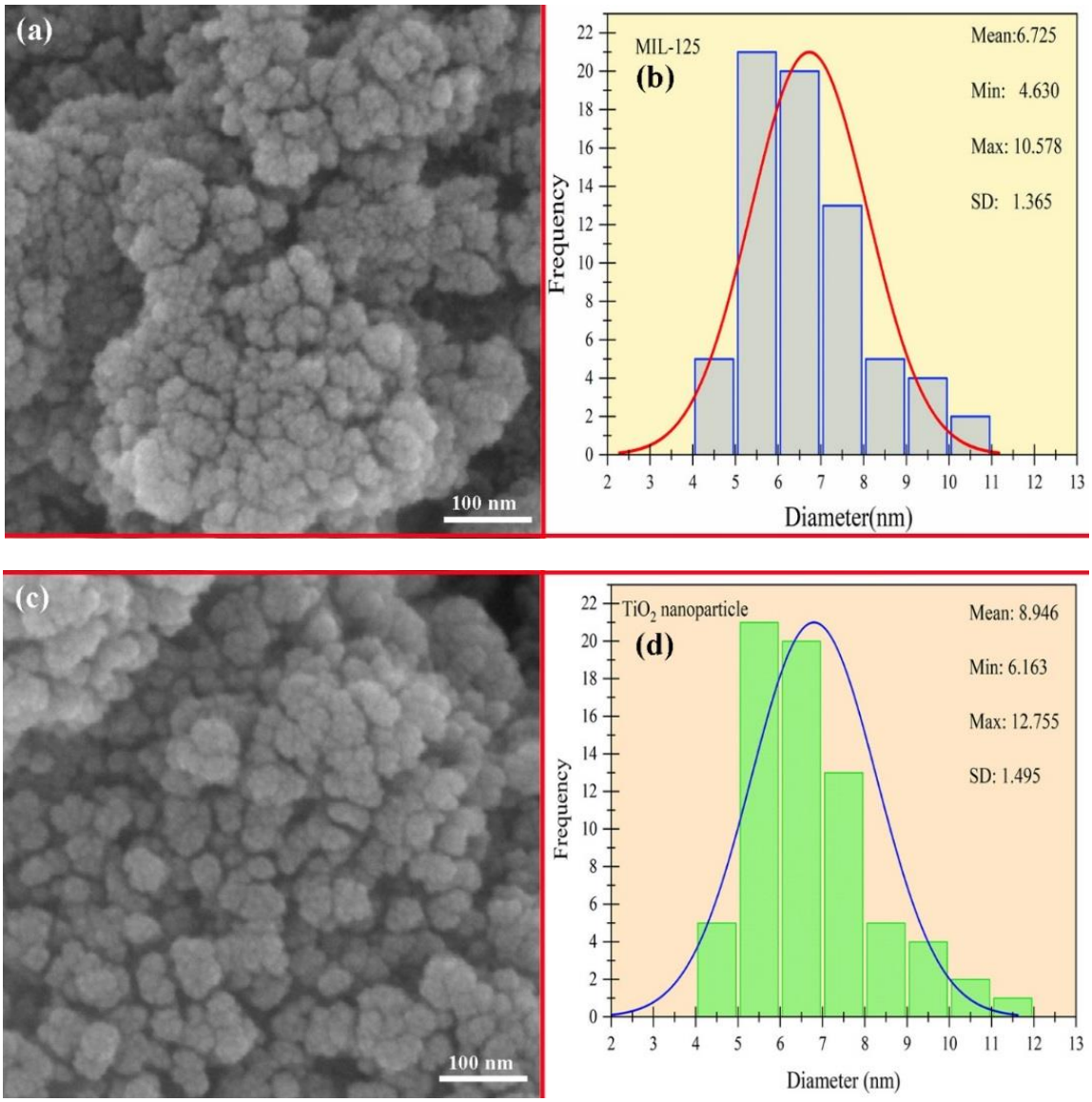

Figure 6. FE-SEM images and particle size distribution of a, b) MIL-125(Ti) and c, d) TiO_2 nanoparticles.

TEM images of the MIL-125(Ti) and TiO_2 NPs are displayed in Figure 7. TEM micrographs confirms an increase in the average particle size as a consequence of the material transformation due to the heat treatment, as shown in the corresponding particle size distribution histograms in Figure 6a and b. MIL-125 crystals exhibited a disordered porous structure. MOF-derived TiO_2 NPs were synthesized in the form of the semi-spherical crystal habits with symmetrical dimensions in the range of 7–12 nm.

The photocatalytic activity of the porous TiO_2 NPs was evaluated in the degradation of reactive blue 21 (RB21), methylene blue (MB), and methylene orange (MO). As seen in Figure 8, the porous TiO_2 NPs possessed a very good ability to degrade organic pigments. UV-vis spectrum and Tauc plot indicated the bandgap of the product to be 3.08 eV that is in the UV region of the electromagnetic spectrum.

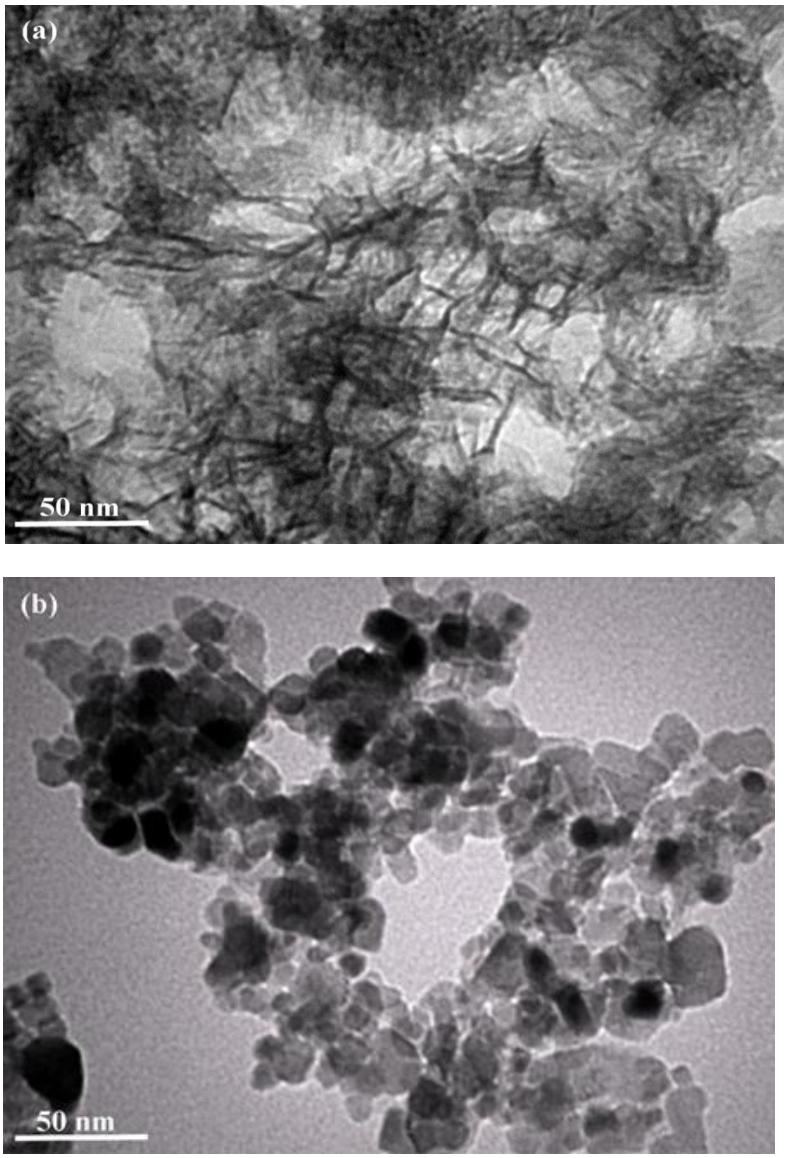

Figure 7. TEM images of (a) MIL-125(Ti) and (b) TiO_2 nanoparticles.

To transfer the electrons from the valance band (VB) to the conduction band (CB), therefore, a source with fewer wavelengths than the visible light is needed. Following this electron transfer, an electron-hole pair generates, subsequently creating an unstable state in the electron structure of TiO_2 NPs, thus extra electrons from CB returns to the VB and electron-hole recombination phenomenon occurs [54]. The electron-hole recombination rate has a direct correlation to the photocatalytic ability. When an adequate amount of oxygen vacancies can capture electrons from TiO_2 semiconductor, the holes can be diffused to the surface of the nanoparticles, leading to the oxidation of the organic dye. A high density of surface oxygen defects is useful for separating the electron–hole pairs. This diminishes the radiative recombination of electrons and holes, and increases the lifetime of the charge carriers, thereby enhancing the photocatalytic activity [57]. Table 1 lists the high surface area of MIL-125 (1023 m^2g^{-1}) and titanium oxide

nanoparticles (163 m^2g^{-1}), and the mesoporous structure obtained from BET porosimetry is a good reason for increasing dye loading capacity and improving the light absorption capacity [55]. Figure 8 shows that the porous TiO_2 nanoparticle is more capable of removing RB21, because the whole of this color has been degraded after 150 min. Table 2 summarizes the photocatalytic ability of TiO_2 NPs to remove these three dyes. The comparative photocatalytic performance of the synthesized MOF-derived titanium oxide along with other photocatalysts reported by other researchers are tabulated in Table 3. It can be observed that the synthesized porous TiO_2 nanoparticles is more efficient than ZnS [53] and ZnO [56, 57] semiconductors for removal of RB21. Also, the currently synthesized TiO_2 exhibited a higher performance for degradation of MB and MO dyes compared to CuS and ZrO_2 photocatalysts [34, 55], as seen in Table 3.

Table 1. The surface area, pore volume and pore size of the porous TiO_2 nanoparticles synthesized in this work.

Sample	BET surface area (m^2g^{-1})	Nitrogen pore volume (cm^3g^{-1})	Pore diameter from BJH analysis (nm)
MIL-125(Ti)	1023	0.447	1.3-3
TiO_2	163	0.374	1.8-3.7

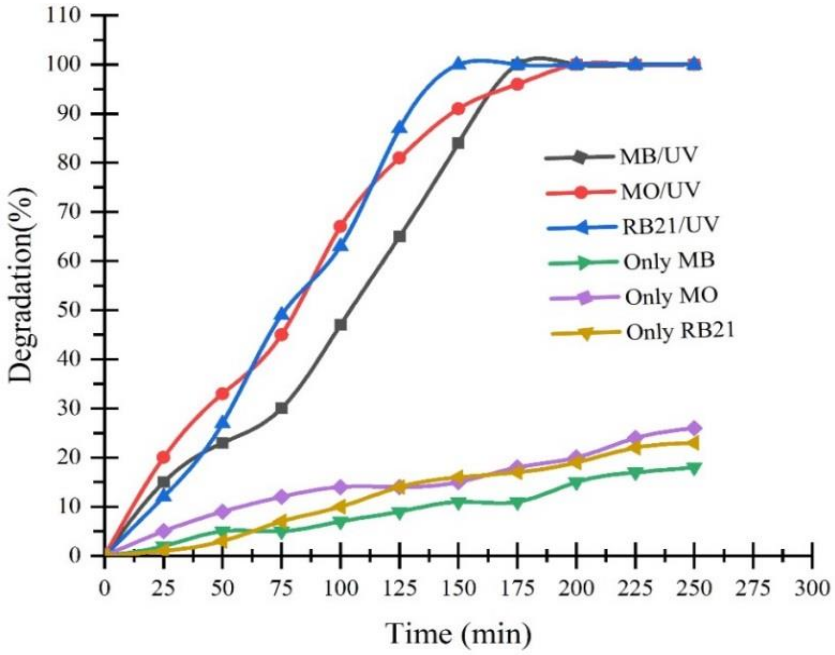

Figure 8. Photocatalytic degradation of MO, MB, and RB21 pigments in the presence of porous TiO_2 nanoparticles.

Table 2. The results of photocatalytic activities of TiO_2 nanoparticles in the degradation of MO/MB/RB21 pigments

Dye	Time (min)	Degradation Level (%)	Photocatalyst
Methylene Orange (MO)	150	91	TiO_2
Methylene Blue (MB)	150	83	TiO_2
Reactive Blue 21 (RB21)	150	100	TiO_2

Table 3. A comparison between photocatalytic performances of the synthesized TiO_2 nanoparticles in degrading MO/MB/RB21 with other research works

Photocatalyst	Dye	Time (min)	Degradation Level (%)	Reference
ZnO	RB21	240	80.3	[56]
ZnO	RB21	240	75	[55]
ZnS	RB21	240	100	[54]
TiO_2 (present work)	RB21	150	100	-
CuS	MB	180	100	[52]
TiO_2 (present work)	MB	175	100	-
ZrO_2	MO	100	61	[57]
TiO_2 (present work)	MO	100	69	-

Conclusions

Porous TiO_2 NPs with an average particle size of 7–12 nm were successfully prepared from the heat treatment of MIL-125(Ti) metal-organic framework intermediate compound at different temperatures. The effect of thermal treatment on the single-phase and high-crystallinity of TiO_2 NPs was evaluated and 500 °C was selected as the optimum temperature for preparation of the anatase phase. The optical studies of the anatase phase of TiO_2 NPs gave the λ_{max}= 364 nm, λ_{em}= 543 nm and E_g = 3.08 eV. High specific surface area (163 m^2g^{-1}) and mesoporous/microporous structure (0.374 cm^3g^{-1} for nitrogen pore volume and 1.8–3.7 nm for pore diameter) of TiO_2 NPs were inherited from MIL-125 structure. These properties caused the light exposure duration to be extended as well as the pigment loading capacity to be increased. Therefore, UV light absorption capacity was significantly increased and consequently, the porous TiO_2 NPs would be able to more effectively remove the RB21, MO, and MB organic pigments.

Acknowledgments

The authors would like to appreciate the Iran's National Elites Foundation for its support from this work.

Disclosure Statement

No potential conflict of interest was reported by the authors.

Orcid

Maisam Jalaly 0000-0002-3123-7460

References

[1]. Lu G., Huang X., Li Y., Zhao G., Pang G., Wang G. *J. Energy Chem*., 2020, **43**:8

[2]. Zhen H.G., Mao H., Ul-Haq I., Li S.H., Ahmad A., Zhao Z.P. *Sep. Purif. Technol.*, 2019, **233**:116042

[3]. Walle M.D., Zhang M., Zeng K., Li Y., Liu Y.N. *Appl. Surf. Sci.*, 2019, **497**:143773

[4]. Du Y., Li G., Chen M., Yang X., Ye L., Liu X., Zhao L. *Chem. Eng. J.,* 2019, **378**:122210

[5]. Li S., Zhang L., Liang X., Wang T., Chen X., Liu C., Li L., Wang C. *Chem. Eng. J.,* 2019, **378**:122175

[6]. Ma C., Li Y., Nian P., Liu H., Qiu J., Zhang X. *Sep. Purif. Technol*., 2019, **229**:115835

[7]. Zhang Y., Ji L., Zheng Y., Liu H., Xu X. *Sep. Purif. Technol.,* 2020, **234**:116124

[8]. Lin Y., Sun Y., Dai Y., Sun W., Zhu X., Liu H., Han R., Gao D., Luo C., Wang X. *Talanta*, 2020, **207**:120300

[9]. Esfahanian M., Ghasemzadeh M.A., Razavian S.M.H. *Artif. Cells, Nanomedicine Biotechnol.*, 2019, **47**:2024

[10]. Ma J., Wang H., Yang X., Chai Y., Yuan R. *J. Mater. Chem. A,* 2015, **3**:12038

[11]. Guan C., Sumboja A., Wu H., Ren W., Liu X., Zhang H., Liu Z., Cheng C., Pennycook S.J., Wang J. *Adv. Mater.*, 2017, **29**:1704117
[12]. Xia H., Zhang J., Yang Z., Guo S., Guo S., Xu Q. *Nano-Micro Lett.*, 2017, **9**:43
[13]. Li Y., Xu Y., Yang W., Shen W., Xue H., Pang H. *Small,* 2018, **14**:1704435
[14]. Adarsh N.N. *Metal–organic framework (MOF)–derived metal oxides for supercapacitors*, In: Dubal D.P., Gomez-Romero P. (Eds.), *Metal Oxides in Supercapacitors*, Elsevier: Amsterdam, 2017, p 165
[15]. Liu Q., Jin L.N., Sun W.Y. *Chem. Commun.*, 2012, **48**:8814
[16]. Li Y., Fu Z.Y., Su B.L. *Adv. Funct. Mater.*, 2012, **22**:4634
[17]. Sajjadifar S., Arzehgar Z., Khoshpoori S. *J. Inorg. Organomet. Polym. Mater.*, 2017, **28**:837
[18]. Sajjadifar S., Arzehgar Z., Ghayuri A. *J. Chin. Chem. Soc.,* 2018, **65**:205
[19]. Meng W., Chen W., Zhao L., Huang Y., Zhu M., Huang Y., Fu Y., Geng F., Yu J., Chen X., Zhi C. *Nano Energy*, 2014, **8**:133
[20]. Lou X.W., Deng D., Lee J.Y., Feng J., Archer L.A. *Adv. Mater.*, 2008, **20**:258
[21]. Liu Y., Wang G., Xu C., Wang W. *Chem. Commun.*, 2002, **2**:1486
[22]. He T., Chen D., Jiao X., Wang Y., Duan Y. *Chem. Mater.*, 2005, **17**:4023
[23]. Maiti S., Pramanik A., Mahanty S. *Chem. Commun.*, 2014, **50**:11717
[24]. Valero-Romero M.J., Santaclara J.G., Oar-Arteta L., van Koppen L., Osadchii D.Y., Gascon J., Kapteijn F. *Chem. Eng. J.*, 360, **2019**:75
[25]. Finegold L., Cude J.L. *Nature*, 1972, **238**:38
[26]. Higashimoto S. *Catalysts*, 2019, **9**:201
[27]. Göltner C.G., Smarsly B., Berton B., Antonietti M. *Chem. Mater.*, 2001, **13**:1617
[28]. Wu M.C., Hiltunen J., Sápi A., Avila A., Larsson W., Liao H.C., Huuhtanen M., Tóth G., Shchukarev A., Laufer N., Kukovecz Á., Kónya Z., Mikkola J.P., Keiski R., Su W.F., Chen Y.F., Jantunen H., Ajayan P.M., Vajtai R., Kordás K. *ACS Nano.*, 2011, **5**:5025
[29]. Misra M., Singh N., Gupta R.K. *Catal. Sci. Technol.*, 2017, **7**:570
[30]. Hu H., Lin Y., Hu Y.H. *Chem. Eng. J.*, 2019, **375**:122029
[31]. Parvizi-Majidi A. *Whiskers and Particulates,* In: Kelly A., Zweben C. (Eds.), *Comprehensive Composite Materials Vol. 1*, Elsevier: Amsterdam, 2000, p 175
[32]. Hamad S., Catlow C.R.A., Woodley S.M., Lago S., Mejías J.A. *J. Phys. Chem. B*, 2005, **109**:15741
[33]. Sabaghi V., Davar F., Fereshteh Z. *Ceram. Int.*, 2018, **44**:7545
[34]. Sabaghi V., Davar F., Sadat-Nabi A., Hasani S. *Int. J. Appl. Ceram. Technol.*, 2019, **16**:2322
[35]. Luttrell T., Halpegamage S., Tao J., Kramer A., Sutter E., Batzill M. *Sci. Rep.*, 2014, **4**:4043
[36]. Wang M., Song G., Li J., Miao L., Zhang B. *J. Univ. Sci. Technol. Beijing Miner. Metall. Mater.,* 2008, **15**:644
[37]. Irie H., Watanabe Y., Hashimoto K. *J. Phys. Chem. B.,* 2003, **107**:5483
[38]. Wang Z., Li X., Xu H., Yang Y., Cui Y., Pan H., Wang Z., Chen B., Qian G. *J. Mater. Chem. A.,* 2014, **2**:12571
[39]. Wei J., Zhao L., Peng S., Shi J., Liu Z., Wen W. *J. Sol-Gel Sci. Technol.,* 2008, **47**:311
[40]. Praveen P., Viruthagiri G., Mugundan S., Shanmugam N. *Spectrochim. Acta A Mol. Biomol. Spectrosc.*, 2014, **117**:622
[41]. Nolan N.T., Seery M.K., Pillai S.C. *J. Phys. Chem. C.,* 2009, **113**:16151
[42]. Venkatasubbu G.D., Ramasamy S., Ramakrishnan V., Kumar J. *Adv. Powder Technol.*, 2013, **24**:947
[43]. Thamarai Selvi T.S., Prasanna A.P.S, Niranjan R., Kaushik M., Devasena T., Kumar J., Chelliah R., Oh D.H., Swaminathan S., Venkatasubbu G.D. *Appl. Surf. Sci.*, 2018, **449**:603

[44]. Khan M., Naqvi A.H., Ahmad M. *Toxicol. Reports,* 2015, **2**:765
[45]. Zhu S.R., Liu P.F., Wu M.K., Zhao W.N., Li G.C., Tao K., Yi F.Y., Han L. *Dalton Trans*., 2016, **45**:17521
[46]. Oveisi M., Asli M.A., Mahmoodi N.M. *J. Hazard Mater.,* 2018, **347**:123
[47]. Dan-Hardi M., Serre C., Frot T., Rozes L., Maurin G., Sanchez C., Ferey G. *J. Am. Chem. Soc*., 2009, **131**:10857
[48]. Azami M.S., Nawawi W.I., Jawad A.H., Ishak M.A.M., Ismail K. *Sains Malaysiana,* 2017, **46**:1309
[49]. Wang H., Yuan X., Wu Y., Zeng G., Chen X., Leng L., Wu Z., Jiang L., Li H. *J. Hazard Mater.,* 2015, **286**:187
[50]. Liang X.X., Wang N., Qu Y.L., Yang L.Y., Wang Y.G., Ouyang X.K. *Molecules*, 2018, **23**:1524
[51]. Yang Z., Xu X., Liang X., Lei C., Cui Y., Wu W., Yang Y., Zhang Z., Lei Z. *Appl. Catal. B Environ*. 2017, **205**:42
[52]. Mathew S., Kumar Prasad A., Benoy T., Rakesh P.P., Hari M., Libish T.M., Radhakrishnan P., Nampoori V.P.N., Vallabhan C.P.G. *J. Fluoresc*. 2012, **22**:1563
[53]. Reyes-Coronado D., Rodríguez-Gattorno G., Espinosa-Pesqueira M.E., Cab C., De Coss R., Oskam G. *Nanotechnol*. 2008, **19**:145605
[54]. Tang R., Xie Z., Zhou S., Zhang Y., Yuan Z., Zhang L., Yin L. *ACS Appl. Mater. Interfaces*, 2016, **8**:22201
[55]. Aflaki M., Davar F. *J. Mol. Liq*., 2016, **221**:1071
[56]. Guerra W.N.A., Santos J.M.T., De Araujo L.R.R. *Water Sci. Technol*., 2012, **66**:158
[57]. Davar F., Majedi A., Mirzaei A. *J. Am. Ceram. Soc*., 2015, **98**:1739

How to cite this manuscript: Vahid Sabaghi, Maisam Jalaly*, Fatemeh Rahnemaye Rahsepar. Photocatalytic degradation of industrial pigments by mil-125 derived porous Titanium Dioxide (TiO_2) nanoparticles. *Journal of Medicinal and Nanomaterials Chemistry*, 2(4) 2020, 300-312. DOI: 10.48309/JMNC.2020.4.4